

# DEGRADATION OF METHYL ORANGE DYE USING TiO<sub>2</sub> IMMOBILIZED IN BIOPOLYMER CHITOSAN UNDER SUNLIGHT IRRADIATION

LAMINE AOUDJIT,\* DJAMILA ZIOUI\* and EL AMINE NEBBAT\*\*

\*Unité de Développement des Equipements Solaires, UDES /Centre de Développement des Energies Renouvelables, CDER, Bou Ismail, 42415, W. Tipaza, Algeria

\*\*Faculty of Sciences, Laboratory LSDME, University of Algiers 1, Algiers, Algeria

✉ Corresponding author: L. Aoudjit, lamineaoudjit@yahoo.fr

Received March 7, 2025

TiO<sub>2</sub>-chitosan beads were prepared and utilized for the photodegradation of methyl orange dye. The characterization of the synthesized TiO<sub>2</sub>-chitosan (CTC) was performed using Fourier transform infrared (FTIR) spectroscopy. The degradation of methyl orange (MO) dyes was ascribed to the improved photocatalytic activity of TiO<sub>2</sub>-chitosan (CTC), supported by techniques such as scanning electron microscopy (SEM), energy dispersive analysis of X-ray (EDAX), and X-ray diffraction (XRD). The experiments on photodegradation were conducted by altering the synergistic effect between TiO<sub>2</sub> and chitosan (CS). Various factors, including initial dye concentration, pH, and catalyst dose, were examined. The findings indicated that a reduction in initial dye concentration and an increase in irradiation time led to a higher percentage of methyl orange dye removal. Experimental data revealed that when exposed to sunlight for 180 minutes, 75.97% of methyl orange was eliminated using TiO<sub>2</sub>-chitosan beads. The best photoactivity was obtained for a concentration of 20 mg/L and a catalyst dose of 0.26 g at pH 9.

**Keywords:** chitosan, nanocomposite TiO<sub>2</sub>, Methyl Orange, advanced oxidation processes

## INTRODUCTION

Methyl orange is a small organic compound featuring two aromatic rings linked by an -N=N double bond. This dye is commonly utilized across various industries, including textile and leather dyeing. As a result of its extensive application, significant quantities of wastewater contaminated with methyl orange are produced. This compound poses health risks, as it can irritate the skin, eyes, and respiratory system. Ingesting methyl orange may lead to internal discomfort, nausea, vomiting, and diarrhea. Additionally, it is harmful to aquatic organisms. Consequently, it is crucial to eliminate methyl orange and other azo dyes from waste streams to reduce their environmental and health effects.<sup>1-5</sup>

Numerous treatment techniques have been devised for the removal of methyl orange, including biological methods, reverse osmosis, membrane filtration, ultraviolet (UV) disinfection, adsorption, photosensitization, solar wastewater treatment (SOWAT), and various chemical approaches. Nonetheless, these techniques frequently come with various drawbacks, inclu-

ding the production of significant sludge and the creation of secondary pollutants.<sup>6-12</sup> Photocatalytic degradation, which utilizes light along with a photocatalyst to decompose chemical substances, has surfaced as a promising approach for the elimination of methyl orange.<sup>13-17</sup> Recently, titanium dioxide (TiO<sub>2</sub>) has become the leading photocatalyst for wastewater treatment applications, attributed to its unique properties. Studies indicate that embedding TiO<sub>2</sub> within a polymer matrix enhances the remarkable stability of this semiconducting material, leading to increased degradation of contaminants compared to using the individual components separately. This approach also addresses some of the drawbacks associated with the use of TiO<sub>2</sub> in polymer films and suspensions, particularly in recovering solid particles. A variety of polymers have been utilized to create membranes, including cellulose acetate (CA), cellulose triacetate (CTA), polysulfone (PSu), polyethersulfone (PES), and polyvinylidene fluoride (PVDF). Additionally, vinylidene fluoride-hexafluoropropylene (PVDF-

HFP) and copolymers such as poly(vinylidene fluoride-trifluoroethylene) (PVDF-TrFE) have also been employed.<sup>18-21</sup>

Chitosan (CS), derived through the deacetylation of chitin, stands out as one of the most fascinating biopolymers and is recognized as the second most prevalent natural polysaccharide among natural polymers. Its appeal lies in its remarkable characteristics, which include high mechanical strength, exceptional chemical resistance, natural occurrence, non-toxicity, ease of production, affordability, biodegradability, thermal stability, and biocompatibility.<sup>5,22-23</sup> These attributes render it suitable for numerous applications, including its use as a biosorbent for the removal of various contaminants, such as heavy metals, dyes, pathogens in wastewater treatment systems.

The inclusion of semiconductor TiO<sub>2</sub> into the primary component CS alters the characteristics of the biopolymer. This study aims to synthesize thin films of TiO<sub>2</sub>-chitosan and apply them for the photocatalytic breakdown of methyl orange dye when exposed to sunlight. Additionally, the assessment of the reusability and stability of the resulting nanocomposite (TiO<sub>2</sub>-chitosan) was conducted.

## EXPERIMENTAL

### Materials and methods

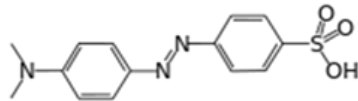
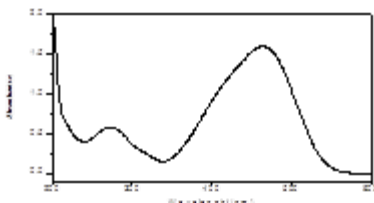
Chitosan was provided by Pelican Biotechnology and Chemical Laboratories, Kerala (India). Titanium dioxide was purchased from Sigma-Aldrich. Acetic acid (99.9% purity) and sodium hydroxide (98% purity) were purchased from Biochem Chemopharma. Table 1 summarizes the properties of methyl orange, which was chosen as a model compound for our flow photocatalysis. All chemicals used in our experiments were of analytical grade.

Solutions of different concentrations (20–40 mg L<sup>-1</sup>) were prepared by diluting the methyl orange stock solution with distilled water. The pH of the solution was adjusted by adding NaOH or HCl.

### Preparation of TiO<sub>2</sub>-chitosan nanocomposite

Titanium dioxide nanoparticles (0.3 g) were mixed with 7.0 mL of 2 wt% chitosan solution (in 2.0% acetic acid) and stirred with a magnetic stirrer at 80 °C for 1 h. The solution mixture was then added dropwise to a cooled sodium hydroxide solution (2 M) using a syringe to form a spherical shape of the beads. The gel beads were further solidified with NaOH solution for 2 h, washed with deionized water to remove the residual NaOH on the surface of the beads and to achieve a neutral pH, and dried in an oven at 60 °C for 6 h. The photocatalytic degradation of methyl orange by the prepared beads was further studied.

Table 1  
Physico-chemical properties of methyl orange (MO)

Name	Methyl orange
Chemical formula	C <sub>14</sub> H <sub>14</sub> N <sub>3</sub> NaO <sub>3</sub> S
IUPAC nomenclature	3,7 diamino-2-8-dimethyl-5 phenylphenazinium chloride
Molar mass (g/mol)	327.34
Solubility	5.20 at 20 °C
λ <sub>max</sub> (nm)	464
Chemical structure	
pKa	3.4
UV/Vis absorption spectrum	

### Characterization

The crystal structure of TiO<sub>2</sub>-chitosan was evaluated by X-ray diffraction (XRD) using a Bruker D8 Discover diffractometer at incident CuKα (40 kV

and 30 mA). The FTIR spectra of the as-prepared TiO<sub>2</sub>-chitosan were recorded using a JASCO-460 plus type FTIR spectrophotometer in the range of 400–4000 cm<sup>-1</sup>; the samples were prepared as KBr pellets under

high pressure. Scanning electron microscopy (SEM) was performed using a Quanta 650 SEM (Thermo Fisher, Waltham, MA, USA) to observe the morphology and microstructure of TiO<sub>2</sub>-chitosan. Elemental analysis was performed by EDAX spectroscopy (Bruker Nano GmbH, Germany).

### Photocatalytic activity experiments

The photocatalytic activity of the prepared photocatalyst TiO<sub>2</sub>-chitosan beads was tested under sunlight using methyl orange (MO) as a pollutant model. For each experiment, 0.26 g of catalyst beads were dispersed in 100 mL of 20 mg/L methyl orange (MO) aqueous solution. Before exposure to sunlight, the suspension was magnetically stirred for 30 min in the dark to ensure adsorption-desorption equilibrium. 5 mL aliquots were taken out at fixed time intervals and centrifuged twice (5000 rpm, 10 min) to separate the solid particles from the solution. According to the Lambert-Beer law, the absorbance of the sample is proportional to the concentration ( $\lambda_{\text{max}} = 464 \text{ nm}$ ); UV-visible spectra were recorded using a double-beam spectrophotometer (Shimadzu UV-1800) and the residual methyl orange (MO) concentration was determined. The photodegradation rate (R) was calculated using the following relationship:<sup>24-25</sup>

$$\text{Degradation}(\%) = \frac{C_0 - C_t}{C_0} \times 100$$

(1)

where  $C_0$  and  $C_t$  are the initial concentration and concentration at time  $t$ , respectively, of methyl orange.

The reusability of the material was also tested. After each run, the TiO<sub>2</sub>-chitosan beads were thoroughly washed with distilled water to ensure that there were no adsorbed molecules and then dried in an oven before its reuse.

## RESULTS AND DISCUSSION

The XRD diffraction patterns of CS and TiO<sub>2</sub>/CS are shown in Figure 1. The peaks at  $2\theta < 25^\circ$  are characteristic of chitosan. Around  $2\theta$  of

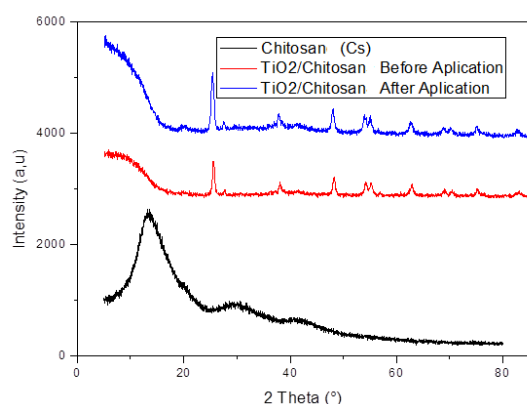


Figure 1: XRD patterns of chitosan and TiO<sub>2</sub>/chitosan composite before and after application

$25^\circ$ , the typical diffraction patterns of TiO<sub>2</sub> anatase and rutile were also found. These peaks are similar to the standard spectra (JCPDS Card No.: 88-1175 and 84-1286). Another peak at  $20^\circ 2\theta$  confirms that TiO<sub>2</sub> is incorporated into the structure of chitosan. These results are in good agreement with those reported in previous work.<sup>5,22-23</sup>

The FTIR spectra of pure CS and TiO<sub>2</sub>/chitosan are shown in Figure 2. The broad band at  $3227.66 \text{ cm}^{-1}$  is attributed to the O-H stretching vibration of adsorbed water. The bands between  $1574$  and  $1024 \text{ cm}^{-1}$  are related to the composition of chitosan. The peaks below  $1000 \text{ cm}^{-1}$  are attributed to Ti-O-Ti bonding, asymmetric stretching modes of Ti-O, and immobilization of TiO<sub>2</sub> on the CS matrix. These results are consistent with those of similar works.<sup>5,22-23</sup>

The surface of the chitosan film is smooth and flat, as shown in Figure 3 (a). The scanning electron microscopy (SEM) image after incorporation of TiO<sub>2</sub> into the chitosan matrix (Fig. 3 (b)) clearly shows that the TiO<sub>2</sub> nanoparticles are uniformly dispersed in the chitosan matrix with some agglomeration. This result confirms the good dispersion of TiO<sub>2</sub> nanoparticles in the CS.<sup>23</sup>

The elemental analyses performed by EDAX confirmed the presence of the elements Ti (14.93%), O (62.29%), and C (22.79%), which are indicative of TiO<sub>2</sub> and chitosan, and can be seen in the EDAX spectra of the TiO<sub>2</sub>-chitosan beads (Fig. 4). The results shown in Figure 4 demonstrated that the chitosan and TiO<sub>2</sub> were combined in an excellent manner.

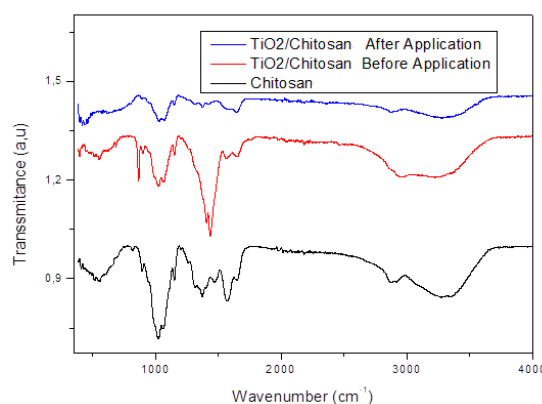
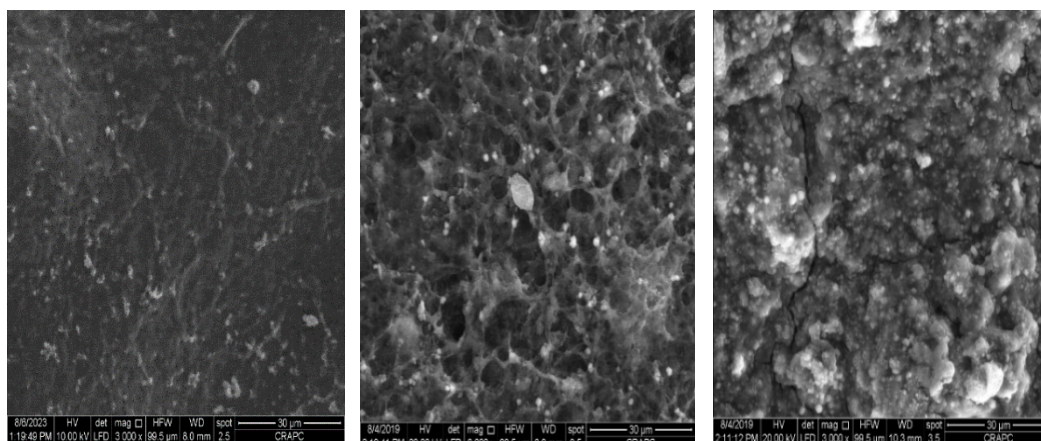
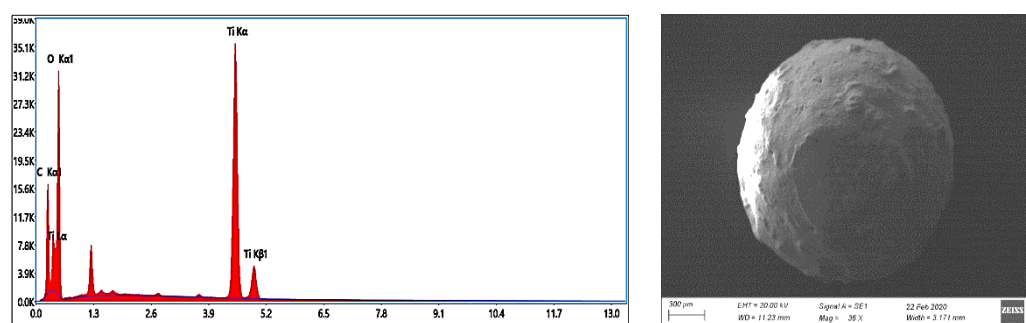


Figure 2: FTIR spectra of pure CS and TiO<sub>2</sub>/chitosan composite before and after application

Figure 3: SEM images of pure CS and TiO<sub>2</sub>/chitosan composite before and after applicationFigure 4: EDX spectrum and mapping of TiO<sub>2</sub>-chitosan composite beads

XRD and FTIR were also used to evaluate the stability of Chitosan/TiO<sub>2</sub> after use. As shown in Figures 1 and 2, no difference was observed between the XRD patterns and FTIR spectra recorded before and after application of the beads, which confirms the stability of the material.

#### Adsorption, photolysis and photocatalysis experiments

Preliminary tests were conducted to evaluate the photocatalytic properties of the materials. Three consecutive experiments were performed to study the degradation process of methyl orange in wastewater: the first one was conducted in the presence of TiO<sub>2</sub>/chitosan catalyst without irradiation (to reveal the adsorption phenomenon); the second one was under light irradiation without TiO<sub>2</sub>/chitosan catalyst (photolysis); and the third one was conducted under light irradiation and in the presence of the suspended TiO<sub>2</sub>/chitosan catalyst (*i.e.*, photocatalysis). Figure 5 shows the degradation process of methyl orange under these three conditions. It can be seen that photocatalysis has a significant effect on the photodegradation of methyl orange (up to 75% of methyl orange is degraded), while the effects of adsorption and

photolysis are negligible (7% and 1%). These results are consistent with the results of previous studies.<sup>24-29</sup> There, the researchers discovered heterogeneous photocatalysis as a method that can oxidize most organic pollutants.<sup>2,30-32</sup>

#### Effect of initial methyl orange concentration

In order to study the effect of the initial pollutant concentration on the photocatalytic degradation performance of methyl orange, we varied its concentration in the range of 20 to 40 mg/L at a pH of 9 and a TiO<sub>2</sub>/chitosan catalyst dosage of 0.26 g. The curves in Figure 6 represent the development of the degradation performance of methyl orange over 180 min at different initial pollutant concentrations. The results show that the lower the initial concentration, the more obvious the degradation of methyl orange. At low substrate concentrations (20 mg/L) and irradiation time of 180 min, the degradation efficiency is as high as about 75.97%, while at initial concentrations of 30 and 40 mg/L, the degradation efficiency drops to 48%. In other words, as the pollutant concentration increases, the degradation performance decreases. Our results are consistent with those reported in other previous works.<sup>2,4-5</sup>

Figure 7 shows the change in the absorption spectrum of methyl orange solutions during the photocatalytic process in the presence of  $\text{TiO}_2/\text{chitosan}$ . The maximum absorption band is located at 464 nm. The decrease in absorption peak at 464 nm is also meaningful with respect to the nitrogen to nitrogen double bond ( $-\text{N}=\text{N}-$ ) of the azo dye, as the most active site for oxidative attack.

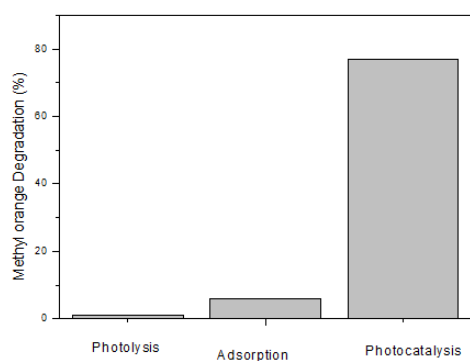


Figure 5: Degradation of methyl orange under different processes ( $C = 20 \text{ mg/L}$ ,  $C_{\text{catalyst}} = 0.26 \text{ g/L}$ , and pH 9)

This indicates a rapid destruction of the chromophore group responsible for the dye's color (the chromophore of methyl orange is broken down and opened up under the attack of  $\text{OH}^\cdot$  radicals). Methyl orange dye decomposes into  $\text{H}_2\text{O}$ ,  $\text{CO}_2$ , and mineral acids. These results are consistent with those of similar works.<sup>2,23</sup>

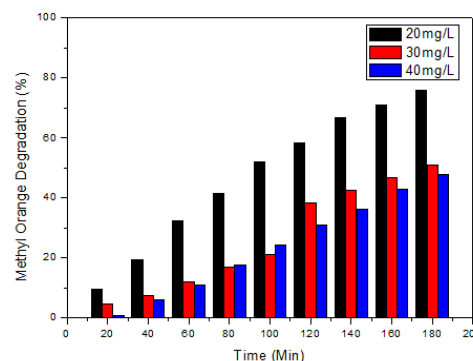


Figure 6: Photodegradation of methyl orange over time at different initial dye concentrations under sunlight (pH 9 and  $C_{\text{catalyst}} = 0.26 \text{ g/L}$ )

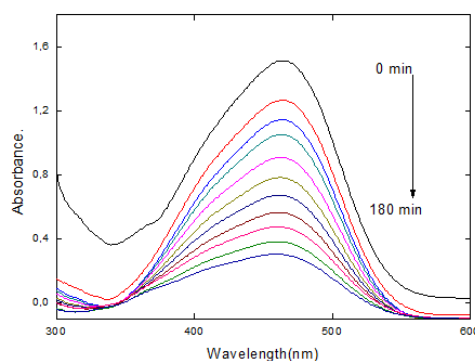


Figure 7: UV spectra of methyl orange at different irradiation times under sunlight ( $C = 20 \text{ mg/L}$ , pH 9 and  $C_{\text{catalyst}} = 0.26 \text{ g/L}$ )

### Effect of initial pH

The entire photocatalytic process is significantly influenced by the pH of the solution, which affects both the surface charge of the catalyst and the chemistry of the pollutants.<sup>17</sup> A successful investigation into the impact of pH on the photodegradation process was conducted using a methyl orange concentration of  $20 \text{ mg.L}^{-1}$ . The pH levels of the methyl orange solution were adjusted between 3 and 13. The results obtained demonstrated that variations in pH value had a substantial effect on the removal efficiency of methyl orange (Fig. 8). The degradation rate is observed to rise with an increase in pH, peaking at pH 9. Beyond this point, further increases in pH

leads to a decline in the degradation rate. Thus, the highest degradation rate occurs within the alkaline range. An alkaline medium promotes the formation of  $\text{OH}^\cdot$  ions, which are crucial for generating  $\text{OH}^\cdot$  radicals, thereby enhancing the rate of photodegradation. The reduction in degradation rate at pH 13 could be attributed to the dissolution of  $\text{TiO}_2/\text{chitosan}$ . Consequently, the optimal pH for the photodegradation of methyl orange is determined to be 9.

### Effect of catalyst dose

Figure 9 illustrates how the quantity of catalysts influences the efficiency of photodegradation. The findings indicate that as



the amount of  $\text{TiO}_2$  rises to 0.26 g, the photodegradation efficiency improves, achieving a removal efficiency of 75.97%. However, when the catalyst amount is increased beyond 0.26 g to 0.52 g, a decline in efficiency is observed. This phenomenon can be understood by noting that the total active surface area grows with the quantity

of catalyst, resulting in a greater number of active sites on its surface. However, after reaching a certain threshold, an increased catalyst dose may become counterproductive due to catalyst aggregation and diminished light scattering, which reduces irradiation.

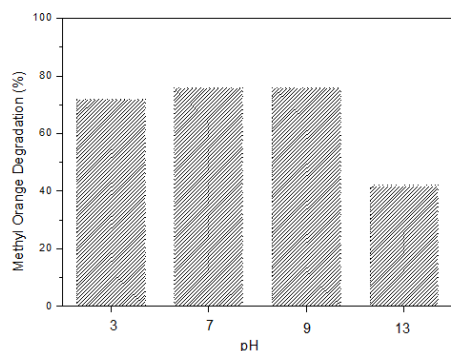


Figure 8: Effect of pH on photodegradation of methyl orange under sunlight ( $C = 20 \text{ mg/L}$ ,  $C_{\text{catalyst}} = 0.26 \text{ g/L}$ )

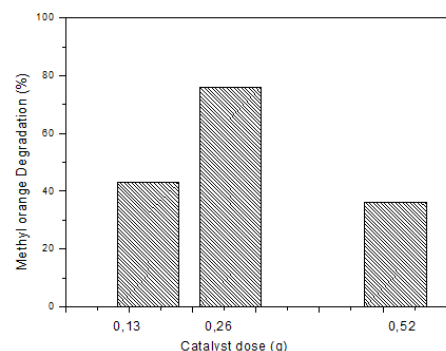


Figure 9: Effect of catalyst dose on photodegradation of methyl orange under sunlight (pH 9 and  $C = 20 \text{ mg/L}$ )

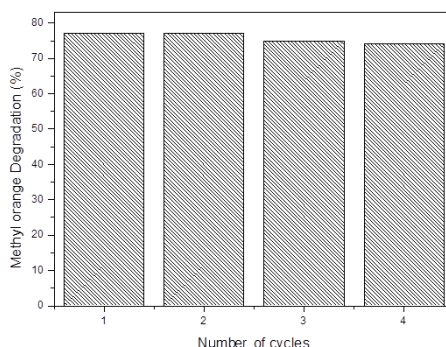


Figure 10: Photodegradation of methyl orange during 4 catalytic cycles in sunlight ( $C = 20 \text{ mg/L}$ ,  $C_{\text{catalyst}} = 0.26 \text{ g/L}$ , and pH 9)

### Reusability of Chitosan/ $\text{TiO}_2$

Recyclability is one of the most important variables in catalysis research.<sup>2</sup> By recycling, the efficiency of the material was tested. After each use, the catalyst was washed with distilled water, and dried in an oven before further use. Figure 10 shows the methyl orange degradation performance of 4 consecutive cycles under the optimized conditions. As shown in Figure 10, the removal efficiency of methyl orange from  $\text{TiO}_2$ -chitosan remained almost unchanged after 4 consecutive cycles.  $\text{TiO}_2$ -chitosan showed a removal efficiency of 75% at the end of the fourth cycle, proving that  $\text{TiO}_2$ -chitosan maintained good photocatalytic degradation performance. This is explained by the stability of CS in aqueous solution and the uniform distribution of  $\text{TiO}_2$

through interaction with CS molecules to ensure effective photocatalytic degradation of methyl orange. These results are consistent with the previous results obtained from XRD, SEM, and FTIR.

### CONCLUSION

The development of efficient photocatalysts for water and wastewater treatment under sunlight irradiation is a promising approach to address the urgent need for water remediation, especially for emerging pollutants, such as methyl orange. Composites based on  $\text{TiO}_2$  and chitosan were prepared and characterized, and their photocatalytic activity for degradation of methyl orange under sunlight irradiation was studied. A maximum degradation efficiency of 75% was

achieved at an initial methyl orange concentration of 20 mg/L, pH 9, and after 3 h of sunlight irradiation. After 4 consecutive applications, the degradation efficiency was constant with a 1% efficiency loss. The produced TiO<sub>2</sub>/chitosan is suitable for water remediation of methyl orange and related emerging pollutants under solar radiation.

**ACKNOWLEDGEMENTS:** This work was supported by the Solar Equipment Development Unit (UDES) Algeria.

## REFERENCES

- <sup>1</sup> Z. Zeffounia, B. Cheknanea, F. Zermane, S. Hanini, L. Aoudjit *et al.*, *Desalin. Water Treat.*, **312**, 187 (2023), <https://doi.org/10.5004/dwt.2023.30008>
- <sup>2</sup> N. Yahia, L. Aoudjit, I. Kahina and I. Baalache, *Cellulose Chem. Technol.*, **58**, 133 (2024), <https://doi.org/10.35812/CelluloseChemTechnol.2024.58.13>
- <sup>3</sup> D. Zioui, L. Aoudjit, F. Touahra and K. Bachari, *Cellulose Chem. Technol.*, **56**, 1101 (2022), <https://doi.org/10.35812/CelluloseChemTechnol.2022.56.98>
- <sup>4</sup> T. Bouarroudj, L. Aoudjit, L. Djahida, B. Zaidi, M. Ouraghi *et al.*, *Water Sci. Technol.*, **83**, 2118 (2021), <https://doi.org/10.2166/wst.2021.106>
- <sup>5</sup> L. Aoudjit, F. Aoudjit, D. Zioui, F. Touahra, D. Halliche *et al.*, *Russ. J. Phys. Chem. A*, **97**, 773 (2023), <https://doi.org/10.1134/S0036024423040040>
- <sup>6</sup> H. Aburideh, Z. Tigrine, D. Zioui, S. Hout, L. Aoudjit *et al.*, *Cellulose Chem. Technol.*, **57**, 911 (2023), <https://doi.org/10.35812/CelluloseChemTechnol.2023.57.80>
- <sup>7</sup> D. Zioui, P. M. Martins, L. Aoudjit, H. Salazar and S. Lanceros-Mendez, *Polymers*, **15**, 1143 (2023), <https://doi.org/10.3390/polym15051143>
- <sup>8</sup> H. Aburideh, Z. Tigrine, L. Aoudjit, Z. Belgroun, K. Redjimi *et al.*, *Cellulose Chem. Technol.*, **55**, 1153 (2021), <https://doi.org/10.35812/CelluloseChemTechnol.2021.55.99>
- <sup>9</sup> S. Igoud, B. Boutra, L. Aoudjit, A. Sebti, F. Khene *et al.*, in *Procs. 7<sup>th</sup> International Renewable and Sustainable Energy Conference (IRSEC)*, 2019, p. 1, <https://doi.org/10.1109/IRSEC48032.2019.9078228>
- <sup>10</sup> S. Igoud, D. Zeriri, L. Aoudjit, B. Boutra, A. Sebti *et al.*, *Irrig. Drain.*, **70**, 243 (2021), <https://doi.org/10.1002/ird.2540>
- <sup>11</sup> B. Boutra, L. Aoudjit, F. Madjene, H. Lebig, A. Sebti *et al.*, in *ACM International Conference Proceeding Series*, 24-26 September, 2015, a13, <http://dx.doi.org/10.1145/2832987.2833008>
- <sup>12</sup> S. Igoud, D. Zeriri, B. Boutra, A. Mameche, Y. Benzegane *et al.*, *Petrol. Sci. Technol.*, **40**, 92 (2022), <https://doi.org/10.1080/10916466.2021.2002358>
- <sup>13</sup> T. Bouarroudj, L. Aoudjit, I. Nessaibia, D. Zioui, Y. Messai *et al.*, *Russ. J. Phys. Chem. A*, **97**, 1074 (2023), <https://doi.org/10.1134/S0036024423050278>
- <sup>14</sup> M. Salima, M. Youcef, T. Bouarroudj, A. Chetoui, I. Belkhettab *et al.*, *Solid State Sci.*, **143**, 107260 (2023), <https://doi.org/10.1016/j.solidstatesciences.2023.107260>
- <sup>15</sup> L. Aoudjit, P. M. Martins, F. Madjene, D. Y. Petrovykh and S. Lanceros-Mendez, *J. Hazard. Mater.*, **344**, 408 (2018), <https://doi.org/10.1016/j.jhazmat.2017.10.053>
- <sup>16</sup> S. Mokhtari, L. Aoudjit, S. Habi Ben Hariz, N. Dokhan and M. Trari, *Russ. J. Phys. Chem. A*, **98**, 2115 (2024), <https://doi.org/10.1134/S0036024424701243>
- <sup>17</sup> L. Aoudjit, D. Zioui, F. Touahra, S. Mahidine and K. Bachari, *Russ. J. Phys. Chem. A*, **95**, 1069 (2021), <https://doi.org/10.1134/S0036024421050034>
- <sup>18</sup> D. Zioui, O. Arous, N. Mameri, H. Kerdjoudj, M. San Sebastian *et al.*, *J. Hazard. Mater.*, **336**, 188 (2017), <https://doi.org/10.1016/j.jhazmat.2017.04.035>
- <sup>19</sup> D. Zioui, L. Aoudjit, Z. Tigrine and H. Aburideh, *Cellulose Chem. Technol.*, **56**, 353 (2022), <https://doi.org/10.35812/CelluloseChemTechnol.2022.56.31>
- <sup>20</sup> D. Zioui, L. Aoudjit, Z. Tigrine, H. Aburideh and O. Arous, *Russ. J. Phys. Chem. A*, **96**, 1334 (2022), <https://doi.org/10.1134/S0036024422060334>
- <sup>21</sup> D. Zioui, H. Salazar, L. Aoudjit, P. M. Martins and S. Lanceros-Méndez, *Polymers*, **12**, 42 (2020), <https://doi.org/10.3390/polym12010042>
- <sup>22</sup> L. Aoudjit, E. A. Nebbat and D. Zioui, *Cellulose Chem. Technol.*, **57**, 437 (2023), <https://doi.org/10.35812/CelluloseChemTechnol.2023.57.39>
- <sup>23</sup> D. Zioui, L. Aoudjit, F. Touahra and K. Bachari, *Cellulose Chem. Technol.*, **56**, 1101 (2022), <https://doi.org/10.35812/CelluloseChemTechnol.2022.56.98>
- <sup>24</sup> T. Bouarroudj, M. Youcef, L. Aoudjit, B. Zaidi, D. Zioui *et al.*, *Water Sci. Technol.*, **89**, 1105 (2024), <https://doi.org/10.2166/wst.2024.054>
- <sup>25</sup> L. Aoudjit, J. M. Queiros, A. S. Castro, D. Zioui, N. G. Ballesteros *et al.*, *Nanomaterials*, **15**, 358 (2025), <https://doi.org/10.3390/nano15050358>
- <sup>26</sup> F. Aoudjit, F. Touahra, L. Aoudjit, O. Cherifi and D. Halliche, *Water Sci. Technol.*, **82**, 2837 (2020), <https://doi.org/10.2166/wst.2020.519>
- <sup>27</sup> F. Ghribi, M. Sehailia, L. Aoudjit, F. Touahra, D. Zioui *et al.*, *J. Photochem. Photobiol. A*, **397**, 112510 (2020), <https://doi.org/10.1016/j.jphotochem.2020.112510>
- <sup>28</sup> A. Sebti, B. Boutra, M. Trari, L. Aoudjit and S. Igoud, in *Procs. International Conference in Artificial Intelligence in Renewable Energetics*, vol. 102, 2020, p. 143, <https://doi.org/10.1007/978-3-030-37207-1>
- <sup>29</sup> F. Saib, F. M. Laoui, L. Aoudjit, F. Touahra, G. Rekhila *et al.*, *Optical Mater.*, **148**, 114806 (2024), <https://doi.org/10.1016/j.optmat.2023.114806>

<sup>30</sup> P. M. Martins, H. Salazar, L. Aoudjit, R. Gonçalves, D. Zioui *et al.*, *Chemosphere*, **262**, 128300 (2021), <https://doi.org/10.1016/j.chemosphere.2020.128300>

<sup>31</sup> L. Aoudjit, H. Salazar, D. Zioui, A. Sebti, P. M. Martins *et al.*, *Polymers*, **13**, 3718 (2021), <https://doi.org/10.3390/polym13213718>

<sup>32</sup> L. Aoudjit, H. Salazar, D. Zioui, A. Sebti, P. M. Martins *et al.*, *Membranes*, **12**, 849 (2022), <https://doi.org/10.3390/membranes12090849>